Current Biology *16*, 945–957, May 23, 2006 ©2006 Elsevier Ltd All rights reserved DOI 10.1016/j.cub.2006.03.058

Article

oko meduzy and Related *crumbs* Genes Are Determinants of Apical Cell Features in the Vertebrate Embryo

Yoshihiro Omori[1] **and Jarema Malicki**[1,*]
[1] Department of Ophthalmology
Harvard Medical School
MEEI, R513
243 Charles Street
Boston, Massachusetts 02114

Summary

Background: Polarity is an essential attribute of most eukaryotic cells. One of the most prominent features of cell polarity in many tissues is the subdivision of cell membrane into apical and basolateral compartments by a belt of cell junctions. The proper formation of this subdivision is of key importance. In sensory cells, for example, the apical membrane compartment differentiates specialized structures responsible for the detection of visual, auditory, and olfactory stimuli. In other tissues, apical specializations are responsible for the propagation of fluid flow. Despite its importance, the role of genetic determinants of apico-basal polarity in vertebrate embryogenesis remains poorly investigated.
Results: We show that zebrafish *oko meduzy* (*ome*) locus encodes a *crumbs* gene homolog, essential for the proper apico-basal polarity of neural tube epithelia. Two *ome* paralogs, *crb2b* and *crb3a*, promote the formation of apical cell features: photoreceptor inner segments and cilia in renal and auditory systems. The motility of cilia is defective following the impairment of *crb2b* function. Apical surface defects in *ome*- and *crb2b*-deficient animals are associated with profound disorganization of neuronal architecture and with the formation of pronephric cysts, respectively. Unexpectedly, despite differences in their structure and expression patterns, *crumbs* genes are, at least partially, functionally interchangeable.
Conclusions: *ome* and related *crumbs* genes are necessary for the formation of gross morphological features in several organs, including the CNS and the renal system. On the cellular level, *crumbs* genes regulate the formation of both ciliary and nonciliary apical membrane compartment.

Introduction

Cell polarity is an essential feature of most eukaryotic cells. A specific form of polarity exists in epithelial structures and is referred to as apico-basal polarity. A characteristic property of epithelial cells, both embryonic and adult, is the subdivision of their surface by a belt of cell junctions into apical and basolateral domains. These two cell-membrane compartments maintain distinct protein and lipid contents, a feature essential for the proper function of most epithelia and for the survival of the entire organism. Secretory and endocytotic pathways are frequently associated with either the apical or the basolateral cell-surface domain and so are cell-cell signaling mechanisms. In addition to epithelial sheets, apico-basal polarity is obvious in highly differentiated tissues, such as those in the nervous system. Similar to epithelia, cell membranes of radial glia, photoreceptors, auditory hair cells, and olfactory sensory neurons are partitioned by a belt of cell junctions into apical and basolateral domains. In *Drosophila* and *C. elegans*, loss of apico-basal polarity is associated with a variety of severe abnormalities, including embryonic lethality, defective organogenesis, and neuronal degeneration.

Several key determinants of apico-basal polarity have been identified during mutagenesis screens for defects in fly and nematode embryogenesis [1–3]. Cloning of mutant loci as well as subsequent analysis of related genes by reverse genetic approaches revealed proteins that specifically localize either to the apical or the basolateral surface of epithelial cells. Currently, at least six proteins are known to localize to the apical surface: Stardust/Nagie oko, Crumbs, Patj, Par-6, aPKC/Heart and Soul, and Par-3/Bazooka. Loss-of-function mutations in the genes that encode these polypeptides frequently lead to defects of junctional complexes and to the loss of apico-basal polarity both in epithelia as well as in highly differentiated cells, such as photoreceptors of the *Drosophila* eye [4–7]. CRB3, Par-6, and some other cell-polarity determinants have been also recently reported to localize to cilia and flagella, which are thought of as a separate apical cell-membrane compartment (reviewed in [8]). In agreement with this observation, the loss of CRB3 activity blocks cilia formation in tissue culture [9]. The relevance of these findings to in vivo conditions has not yet been tested.

In the context of vertebrate embryogenesis, epithelial polarity pathways have been studied most extensively in zebrafish. Genetic screens in this model organism revealed a group of loci that function as determinants of apico-basal polarity ([10] and references therein). Their mutant phenotypes have been mainly analyzed in neural tube epithelia, where they produce a displacement of apically localized structures, such as cell junctions and centrosomes to more basal regions [11–15]. Cloning of mutant loci revealed a close relatedness between vertebrate neuroepithelial polarity pathways and mechanisms that regulate the polarity of fly embryonic epithelia. Thus, the zebrafish *nagie oko* (*nok*) gene is homologous to *stardust*, while *heart and soul* (*has*) is homologous to *DaPKC* [11, 14]. Zebrafish *ncad* and *mosaic eyes* (*moe*) loci are related to *shotgun* and *yurt*, respectively [12, 15, 16]. Although the function of several constituents of apico-basal polarity pathways has been characterized in the vertebrate embryo, the role of other key determinants, including the *crumbs* genes, remains unknown.

We report that the zebrafish *oko meduzy* (*ome*) locus encodes a transmembrane protein homologous to the

*Correspondence: jarema_malicki@meei.harvard.edu

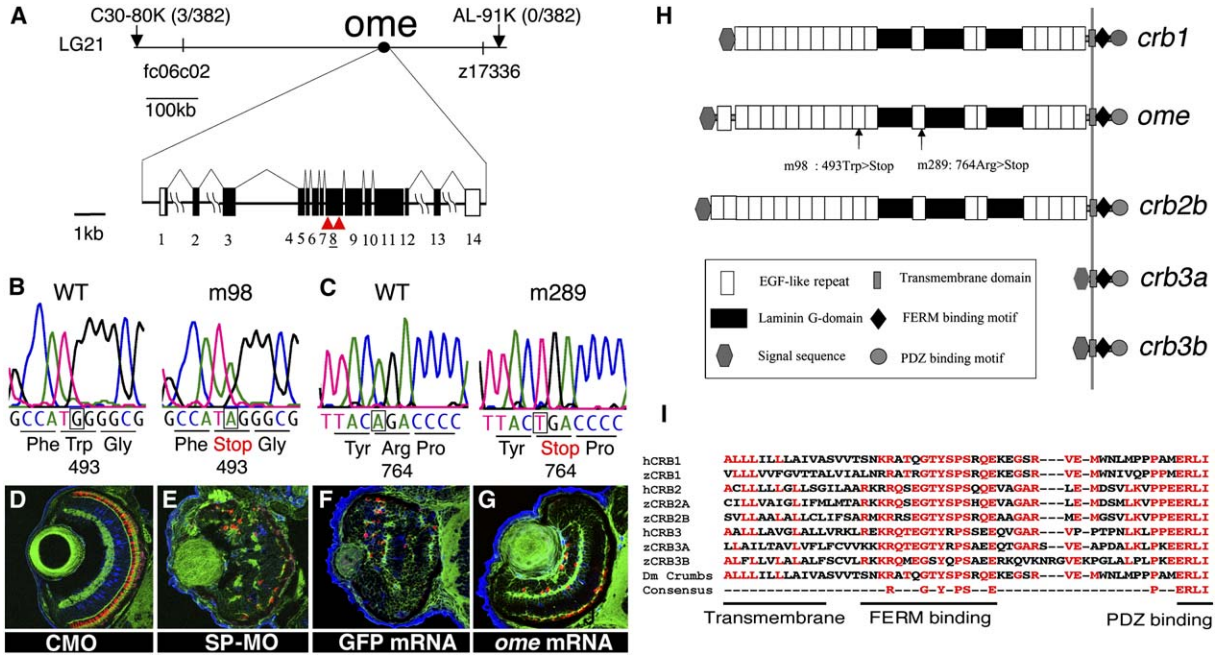

Figure 1. The *oko meduzy* Gene Encodes a Zebrafish *crb* Homolog

(A) A genetic map of the *ome* genomic region and exon/intron structure of the *ome* transcript. The positions of defects in the ome^{m98} and ome^{m289} mutant alleles are indicated (red arrowheads).

(B and C) A comparison of sequence trace data for wild-type and mutant alleles. Both mutations introduce premature termination codons, which truncate the Ome polypeptide far upstream of its transmembrane domain.

(D–G) The phenocopy and rescue of neuronal patterning defects in *ome* animals. Transverse cryosections through embryonic retinae stained with phalloidin to visualize plexiform layers (green), the zpr-1 antibody to visualize double cones (red), and anti-carbonic anhydrase to visualize Muller glia (blue). Retinal lamination is fully formed in control morpholino-treated embryos at this stage (D). The injection of anti-*ome* morpholino induces neuronal architecture defects that closely resemble the ome^{m98} phenotype (E). The injection of *ome* mRNA (G), but not GFP mRNA (F), rescues neuronal architecture in ome^{m98} mutants.

(H) A schematic diagram of zebrafish Crumbs polypeptides. The N-terminal signal peptides, EGF-like repeats, Laminin G domains, transmembrane regions, and the FERM and PDZ binding motifs in the cytoplasmic tails are indicated. The positions of the ome^{m98} and ome^{m289} mutation sites are indicated with vertical arrows.

(I) Comparison of Crumbs C termini from zebrafish, human, and *Drosophila*. Residues identical in at least 5 out of 9 sequences are in red. Invariant residues are indicated in the consensus sequence.

Additional data are presented in Figure S1.

fly *crumbs*. *ome* mutations produce a severe basal displacement of cell junctions in neuroepithelial cells. An *ome* paralog, *crb2b*, is essential for the size determination of the apical membrane domain in photoreceptor cells. *crb2b* and another *ome* paralog, *crb3a*, also determine the size of another apical feature, the length of cilia in renal and auditory systems, respectively. These data indicate that vertebrate *crumbs* genes share a common role in the formation of the apical cell-membrane domain, frequently by regulating its size in both the ciliary and the nonciliary compartment. The absence of their function causes a misplacement or a reduction of diverse apical surface features and is accompanied by profound defects in embryogenesis.

Results

The Zebrafish *ome* Locus Encodes a Homolog of *Drosophila crumbs*

The *ome* locus was identified in a large-scale mutagenesis screen for defects in zebrafish embryogenesis [17, 18]. The initial analysis of the *ome* phenotype revealed a profound neuronal patterning defect in the zebrafish retina [13]. To localize the mutant gene, we identified an *ome*-linked AFLP polymorphism. By using a reference map cross, we mapped *ome* to linkage group 21. Subsequent analysis with an F2 mapping panel revealed three recombination events in 382 meioses between the SSLP polymorphism C30-80K and the *ome* locus and no recombination between *ome* and the SSLP AL-91K (Figure 1A). Since the *ome* mutant phenotype is similar to that of *nagie oko* (*nok*) and polypeptides encoded by both vertebrate and invertebrate *nok* homologs bind to Crumbs protein [7, 19], we hypothesized that zebrafish *crumbs* genes are strong candidates for the gene responsible for the *ome* phenotype. By comparing our mapping results with data available in public databases, we found that a *Drosophila crumbs* homolog maps to the vicinity of the *ome* locus.

We cloned the full-length cDNA of the *crumbs* homolog that maps to the *ome* genomic region by means of 5′ and 3′ RACE, and we identified an ORF of 1466 amino acids. Sequencing of this gene from mutant animals revealed that the ome^{m98} and ome^{m289} alleles carry single base pair substitutions that introduce stop codons at amino acid positions 493 and 764, respectively (Figures 1A–1C), and result in a loss of C-terminal sequences, including the transmembrane region and the cytoplasmic

tail. These truncations most likely result in a complete loss of function.

The closest *ome* homolog in the mouse is *Crb2*. To test whether or not the gene responsible for the *ome* defect has been correctly identified, we phenocopied the *ome* defect by morpholino knockdown. The injection of either ATG-directed or splice site (SP)-directed anti-*crumbs* morpholinos produces a phenotype that closely resembles *ome* mutants, including the disruption of eye pigmentation and a severe disorganization of retinal architecture (Figure 1E, see also Figure S1B in the Supplemental Data available with this article online). At 3 dpf, 71% of ATG and 84% of SP morpholino-injected fish display abnormal eye pigmentation that characterizes *ome* mutants (Table S1). To further confirm the identity of *ome*, we carried out rescue of its phenotype. The full-length *crumbs* mRNA was injected into embryos obtained from crosses between ome^{m98} heterozygotes, and eye pigmentation as well as retinal pattern were evaluated in genotypically mutant embryos 72 hpf. After *ome* mRNA injection, less than 4% of embryos display abnormal eye pigmentation, a significant difference compared to 27% in a control GFP mRNA-treated population (Table S1; Figure S1D, compare to Figure S1C). In addition, the gross features of retinal architecture form correctly in ~50% of *ome* homozygotes treated with *ome* mRNA (Figure 1G, Table S1). By contrast, all of the GFP mRNA-treated *ome* mutant homozygotes display severely disorganized retinae (Figure 1F, Table S1). These results provide convincing evidence that the *ome* defect is due to mutations in a zebrafish *crumbs* homolog.

Several *crumbs* Genes Are Present in the Zebrafish Genome and Display Diverse Expression Patterns

Although three *crb* homologs, *CRB1*, *CRB2*, and *CRB3*, are known in mammalian genomes, no zebrafish *crumbs* genes have been described so far. By searching zebrafish genomic databases, we identified partial sequences of five genes homologous to *crb*, and by means of 5′ and 3′ RACE, we isolated their full-length cDNA sequences. Based on sequence comparisons, we conclude that one of these genes is homologous to mammalian *CRB1*, two to *CRB2*, and the remaining two to *CRB3* (Figures 1H and 1I and Figure S1G). The full-length zebrafish *crb1* cDNA contains an ORF of 1428 aa, and its protein product features 19 EGF-like repeats and 3 laminin-G domains. Two other zebrafish *crb* genes, *ome* and *crb2b*, encode ORFs of 1466 and 1458 amino acids, respectively. The Ome and Crb2b polypeptides contain 20 and 21 EGF-like repeats, respectively, and each features 3 laminin-G domains. Finally, two zebrafish genes, *crb3a* and *crb3b*, are homologous to *CRB3*. In contrast to other Crb polypeptides, the *crb3* gene products contain very short extracellular domains (Figure 1H), and their full-length ORFs are only 109 and 96 amino acids long in *crb3a* and *crb3b*, respectively. Crb cytoplasmic tails are highly conserved and, similar to the fly protein, include a FERM binding motif and a PDZ binding sequence (Figures 1H and 1I) [5, 20].

The zebrafish *crumbs* genes display diverse expression patterns (Figure S2). *crb1*, *ome*, and *crb2b* are mostly expressed in the central nervous system. The first two of these genes display complex expression patterns in the brain and the retina. *crb2b*, on the other hand, is almost exclusively expressed in photoreceptor cells, both in the retina and in the pineal gland (Figures S2G and S2I). Outside the central nervous system, *crb2b* is expressed in the pronephros. In contrast to the above three loci, *crb3* genes are not expressed in the CNS. *crb3a* transcript is present at a high level in the otic vesicle, and the expression of both *crb3* genes is also detectable in the digestive tract primordium. These varied expression patterns suggest that the *crumbs* genes play diverse developmental roles.

ome Is a Determinant of Apico-Basal Polarity

Consistent with the *ome* neuroepithelial phenotype [13], Crumbs immunostaining is observed in the eye neuroepithelium in the apical region of the cell membrane, and at 30 hpf, it is particularly enriched in the area immediately apical to the adherens junction (AJ)-associated actin bundles (Figures 2A–2A″, arrows). A very similar distribution is also present in the brain (Figure 2A, arrowhead). Based on the results of in situ hybridization experiments, immunostaining in the retinal neuroepithelium most likely corresponds to the Ome polypeptide. In ome^{m98} mutant retinae at the same stage, foci of actin bundles form ectopically (Figures 2B–2B″). Staining with antibodies to β-catenin and ZO-1 reveals that these ectopic foci display molecular characteristics of cell junctions (Figures 2H–2H″, Figures S3B–S3B″, S3D). As one would expect, in ome^{m98} mutant animals, they do not, however, display Crumbs immunoreactivity (Figures 2B and 2B″). To visualize the shape of cells in wild-type and in *ome* retinal neuroepithelia, we expressed GFP in a subset of neuroepithelial cells. Mutant cells appear to be rounder, relative to their wild-type counterparts (Figure S3F, compare to Figure S3E). At later stages of embryogenesis, *ome* mutations cause opsin misdistribution throughout the entire photoreceptor cell membrane (described in Supplemental Data, and data shown in Figure S4).

Although the brain of ome^{m98} mutant homozygotes is characterized by somewhat aberrant shape and its ventricular lumen occasionally appears to be reduced, mutant forebrain and midbrain neuroepithelia appear grossly normal at 30 hpf. Immunostaining for β-Catenin, ZO-1, Has/aPKC, and Pard3, all components of either cell junctions or the apical cell-surface domain, does not reveal obvious defects in the brain neuroepithelium (Figures 2D, 2F, and 2H; Figure S3B). As both *ome* and *crb1* are expressed in the brain neuroepithelium, genetic redundancy of these two loci would seem to be one likely explanation for the lack of obvious defects in the *ome* mutant brain. A morpholino knockdown of *crb1* in *ome* mutant animals does not, however, produce an obvious brain phenotype either (data not shown).

To gain insight into the mechanism underlying the mutant phenotype, we asked whether the absence of *ome* function affects the distribution of other apical determinants of cell polarity. Our previous studies revealed that the Nok polypeptide is absent in the vicinity of ectopic junctions in ome^{m98} mutant homozygotes [14]. To extend this analysis, we evaluated the distribution of Has/aPKC and Pard3. In the wild-type neuroepithelium, aPKC immunoreactivity partially overlaps with junctional complexes and at the apical surface displays the

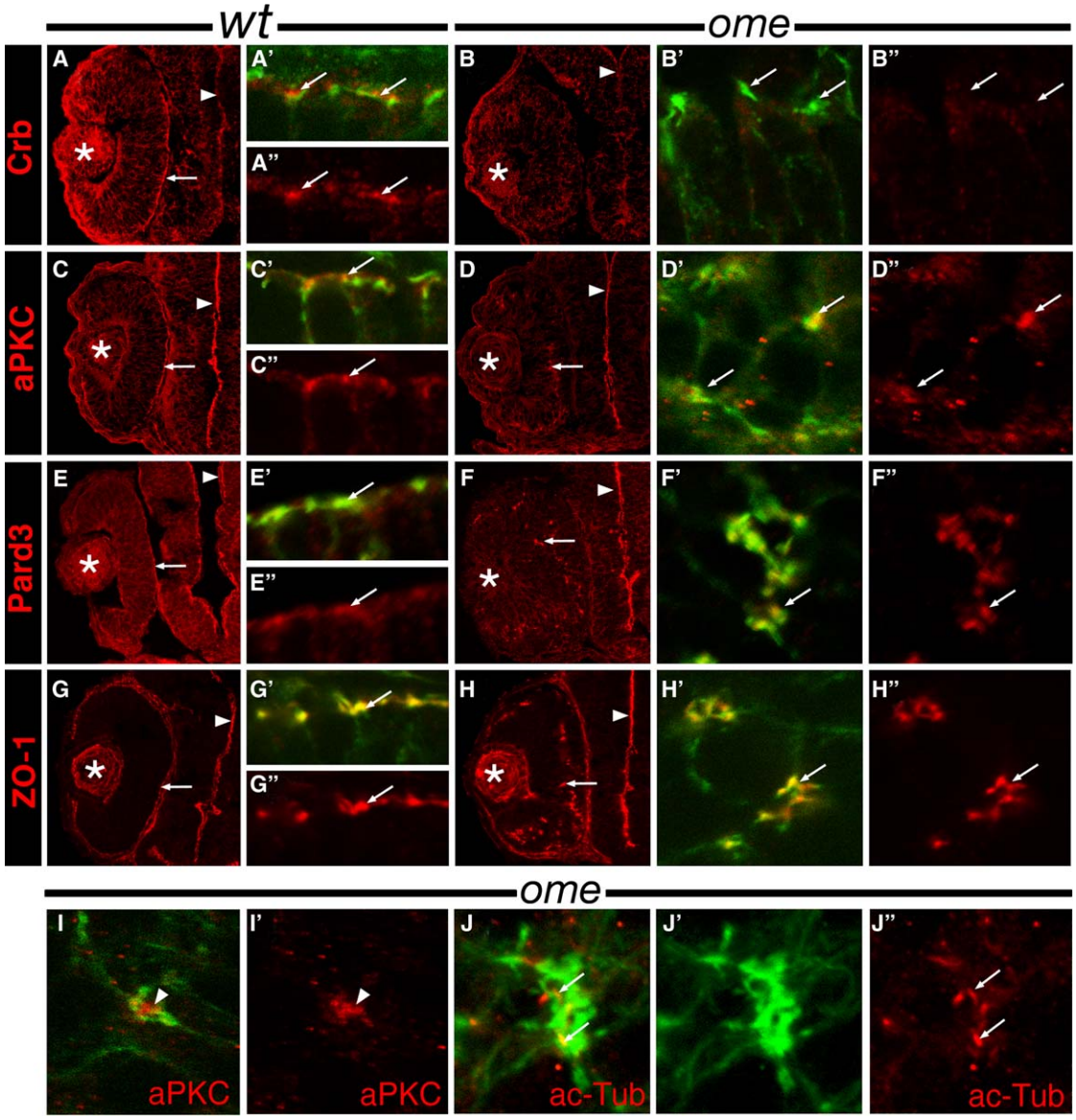

Figure 2. Apical Determinants Are Mislocalized in *ome* Mutants

Transverse sections through wild-type or mutant retinae. In (A)–(H), the left-most panels show the entire eye at 30 hpf, while middle and right panels, marked (′) or (″), present higher magnifications of staining patterns. The determinants of apico-basal polarity are visualized by immunostaining (red). Cell junction-associated actin bundles are visualized with phalloidin (green). Arrows indicate cell junctions, arrowheads point to the brain ventricle, and asterisks mark the lens.

(A–A″) Crumbs expression and adherens junction-associated actin bundles in the wild-type. High concentration of Crb staining is found apically (arrows), in the immediate vicinity of adherens junctions.

(B–B″) Crumbs expression and adherens junction-associated actin bundles in *ome* mutant retina. Adherens junction-associated actin bundles (green) are misplaced to ectopic positions (arrows in [B′]). Crb signal is absent (B″).

(C–C″) Has/aPKC immunoreactivity at the apical surface of the wild-type neuroepithelium partially overlaps with cell junctions.

(D–D″) In *ome* mutant retinae, Has/aPKC staining is confined to the vicinity of ectopic adherens junctions.

(E–E″) In the wild-type, Pard3 immunoreactivity colocalizes with cell junctions at the apical surface.

(F–F″) In *ome* mutant retinae, Pard3 staining is confined to ectopic adherens junctions.

(G–G″) ZO-1 staining colocalizes with actin staining in the wild-type retina.

(H–H″) This is also the case in *ome* mutant retinae.

(I–I′) In *ome* mutant retinae at 28 hpf, aPKC-positive areas (red, arrowhead in [I′]) are occasionally encircled by adherens junctions (green, [I]).

(J–J″) In *ome* mutant retinae at 30 hpf, cilia (red, [J″]) localize to the immediate vicinity of ectopic junctions (green, [J′]). In some cases, they appear embedded in junctional complexes (arrows).

Additional data are presented in Figures S3 and S4.

highest intensity in the vicinity of junctions (Figure 2C′; Figure S3C). Pard3 immunoreactivity, on the other hand, appears to be largely confined to cell junctions (Figures 2E–2E″). In contrast to Nok, both Has/aPKC and Pard3 remain localized to ectopic junctions in mutant retinae (Figures 2D–2D″, 2F–2F″).

An additional indication that the ectopic junctional complexes of *ome* retinae retain apical characteristics is the localization of cilia. In wild-type retinal neuroepithelia, cilia localize to the apical surface [13, 21] (Movies S1 and S3). Similarly, in *ome* mutant retinae, nearly 70% (n = 80) of cilia appear to be in physical contact with ectopic phalloidin-positive areas when viewed on optical sections, and in some cases cilia appear to be embedded within junctional complexes (Figures 2J–2J″, Movies S2 and S4). These data demonstrate that in the *ome* mutant neuroepithelium, the apical surface displays gross morphological abnormalities.

crb2b Is a Determinant of Apical Surface Size in Photoreceptors

Similar to epithelial cells, the photoreceptor cell membrane is partitioned into apical and basolateral domains by a belt of cell junctions, which for historical reasons is called the outer limiting membrane (OLM) [22]. Immunostaining reveals that Crumbs polypeptide(s) localize immediately apical to the OLM (Figures 3A–3E), suggesting a role in the specification of apical membrane. Based on in situ hybridization data (Figure S2), the immunoreactivity in photoreceptor cells appears to be contributed mostly by the *crb2b* gene. To determine whether or not *crb2b* is involved in photoreceptor morphogenesis, we knocked down its function with anti-ATG-directed (ATG) and anti-splice site-directed (SP; Figure 3O) morpholino oligonucleotides. Morpholino knockdown results in the complete or near-complete loss of the *crb2b* transcript (Figure S6H) and a strong reduction of Crumbs immunoreactivity in the photoreceptor cell layer (Figure S5B, compare to Figure S5A). The residual Crumbs signal that persists in morphant photoreceptors is most likely contributed by the *ome* gene. *crb2b* knockdown also produces a pronounced decrease of Nok staining (Figure S5D, compare to Figure S5C), suggesting that Crb2b and Nok polypeptides interact at the apical surface of vertebrate photoreceptors. In contrast to Nok, Has/aPKC staining is not obviously affected in *crb2b* morphants (Figure S5F, compare to Figure S5E). This is consistent with the observation that Has/aPKC continues to localize to ectopic cell junctions in *ome* mutant neuroepithelium.

To study photoreceptor morphology in *crb2b* morphants, cryosections of larvae at 5 dpf were stained with the zpr-1 antibody, which labels double cones [23]. Although the retinal layering of *crb2b* morphants is fully developed, photoreceptor morphology is different from that in control animals. In wild-type photoreceptors at 5 dpf, the inner segment, defined as the area apical to the OLM and basal to the outer segment, accounts for ~50% of photoreceptor cell length, defined by the apico-basal extent of Zpr-1 staining (Figure 3F, quantitated in Figure 3P). In contrast to that, the inner segments of *crb2b* morphants are clearly shorter, accounting for only 15%–30% of photoreceptor length (Figures 3G, 3H, 3P, and 3Q). Measurements of inner segment length on electron micrographs produced similar results (Figure 3Q). The inner segment length recovers when *crb2b* mRNA is injected along with the anti-SP morpholino (Figures 3I and 3Q), indicating that inner segment shortening is not due to a nonspecific toxicity. These observations suggest that *crb2b* determines the apical membrane size in the photoreceptor cell.

As the photoreceptor cell differentiates, its inner segment size increases from ~20% to 50% of the total photoreceptor length (Figure 3J, compare to Figure 3F, quantitated in 3P). A reduction of the apical cell-membrane size in morphant animals may thus reflect a general role of *crb2b* in photoreceptor maturation. To investigate whether or not this is the case, we evaluated two other photoreceptor features: inner segment staining pattern and the differentiation of synaptic termini. The inner segment of mature photoreceptors contains a round area of weaker Zpr-1 immunoreactivity, which most likely corresponds to a cluster of mitochondria (Figures 3F and 3L, arrow). The frequency of this staining pattern increases during photoreceptor differentiation, from ~40% at 3 dpf to roughly 80% at 5 dpf (Ex3 in Figure 3P). In *crb2b* morphants at 5 dpf, the Zpr-1 negative area is observed in approximately 70% of inner segments (Figure 3P). The shape of synaptic termini is another indicator of photoreceptor maturity (Figures 3F and 3N, horizontal bracket). The frequency of cone-shaped synaptic pedicles increases from roughly 30% at 3 dpf to nearly 90% at 5 dpf in control morpholino-treated zebrafish (Figure 3P). Similar to control embryos, in *crb2b* morphants, over 70% of photoreceptors feature cone-shaped pedicles at 5 dpf. This result is corroborated by the analysis of synaptic termini on electron micrographs (Figure S6, described further in Supplemental Data). Thus by several criteria, photoreceptor differentiation is only slightly delayed in *crb2b* morphants (appx. half a day, assuming a linear increase in the frequency of either feature), indicating that *crb2b* does not play a general role in photoreceptor maturation and instead functions as a determinant of apical surface area.

crb2b Is Necessary for the Differentiation and Motility of Renal Cilia

In addition to the staining of apical cell membranes in the nervous system, we found strong Crumbs immunoreactivity in a subset of cells that form pronephric tubules and ducts (Figures 4A, 4C–4E). In the pronephric system, a subset of cells differentiates dense bundles of cilia at the apical surface. At 4 dpf, these cells, but not their neighbors, display intense apical Crumbs immunostaining (Figures 4D and 4E). Two observations suggest that this staining is contributed by the *crb2b* gene. First, only *crb2b* transcript is detected by in situ hybridization in the pronephros (Figure S2I′). Second, *crb2b* morpholino knockdown produces a strong reduction or the absence of Crumbs immunoreactivity in pronephric epithelia (Figure 4B, compare to Figure 4A).

To analyze *crb2b* function in the pronephros, we treated zebrafish embryos with anti-*crb2b* ATG and SP morpholinos. The treatment with either reagent produces pronephric tubule cysts (Figure 4G, compare to Figure 4F) and a dilation of pronephric ducts (Figure 4I, compare to Figure 4H). At 4 dpf, ~60% of ATG and 65% of SP morphants display kidney cysts, compared to about 1% in control morpholino-treated animals (Figure 4P). The kidney cyst phenotype is rescued by *crb2b* RNA coinjection (Figure 4P). As Crumbs immunoreactivity suggests that *crb2b* may play a particularly prominent role in ciliated cells, we investigated pronephric

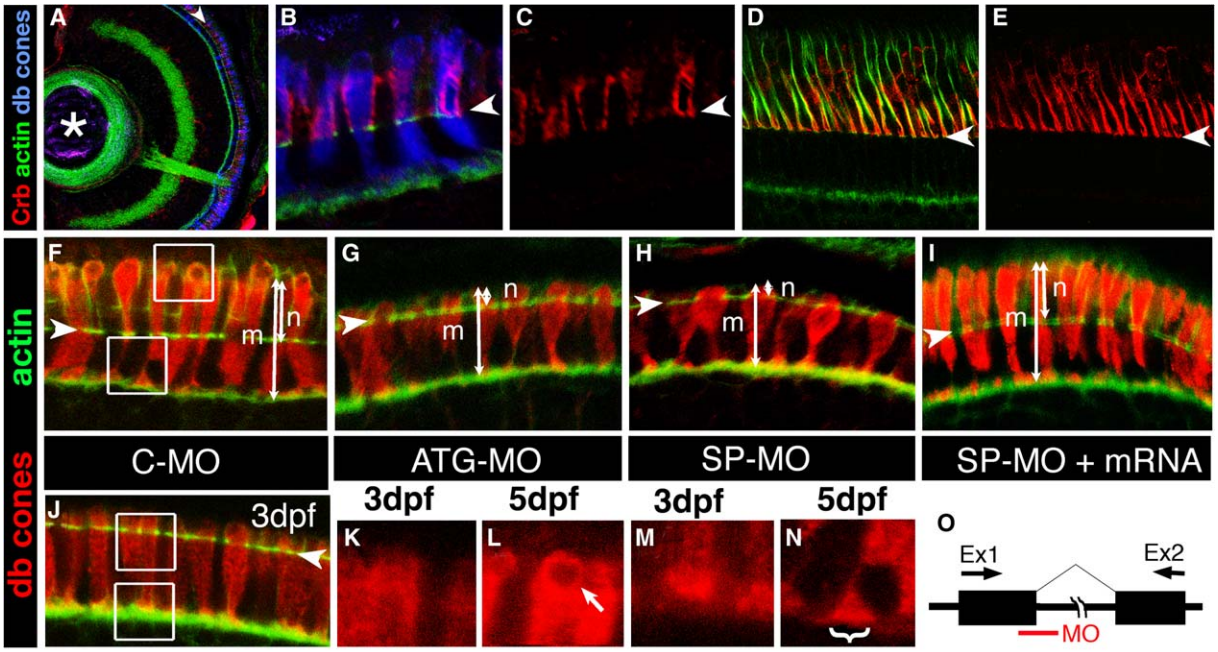

P

	IS length			Synapse shape	IS staining
	Ex1	Ex2	Ex3		
C-MO 3dpf	-	-	22±5	30±15	40±23
C-MO 4dpf	-	-	40±6	54±17	53±23
C-MO 5dpf	48±5	59±9	55±6	88±21	83±12
ATG-MO	16±4	29±12	-	-	-
SP-MO	26±6	19±6	30±4	74±11	69±13
SP-MO+mRNA	-	47±8	44±8	-	-
C-MO+mRNA	-	-	49±3	-	-

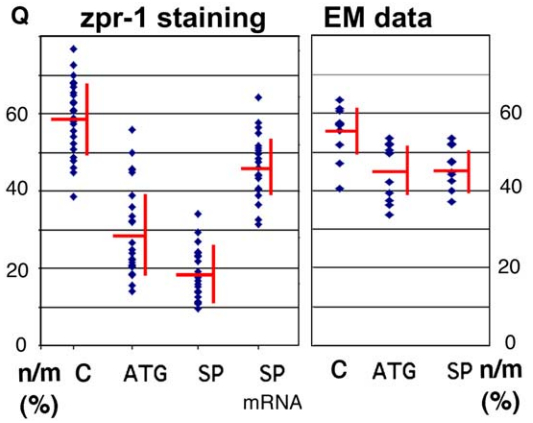

Figure 3. *crb2b* Specifies Apical Membrane Size in Photoreceptor Cells

(A–E) Subcellular localization of Crumbs in photoreceptors. Transverse cryosections through the retina were stained with phalloidin to visualize plexiform layers and cell junctions (green), zpr-1 antibody to visualize double cones (blue), and anti-Crumbs antibody (red). Crb staining is present in the photoreceptor inner segment, immediately apical to the cell junctions of the outer limiting membrane (arrowheads) in the larval retina at 5 dpf (A–C) as well as in the adult (D, E).

(F–J) Transverse cryosections through retinae of morpholino-treated larvae stained with Zpr-1 antibody to visualize double cones (red) and phalloidin to visualize actin filaments (green).

(F) Control morpholino-treated retina. The length of the photoreceptor inner segment (n) and the length of the entire photoreceptor cell (m) are indicated with arrows.

(G and H) Photoreceptor inner segments are shortened in the retinae of *crb2b* ATG (G) and *crb2b* SP (H) morpholino-treated animals.

(I) Coinjection of *crb2b* mRNA with *crb2b* SP morpholino restores the wild-type phenotype.

(J) At 3 dpf, photoreceptor inner segments are short and synapses are morphologically immature.

(K) Detail of (J). At 3 dpf, the photoreceptor inner segment is uniformly labeled.

(L) Detail of (F). At 5 dpf, a round area of weaker staining (arrow) forms in the photoreceptor inner segment.

(M) Detail of (J). At 3 dpf, photoreceptors display blunt synaptic termini.

(N) Detail of (F). At 5 dpf, photoreceptors display triangle-shaped synaptic termini (horizontal bracket).

(O) The efficiency of the *crb2b* SP-MO knockdown was monitored by RT-PCR with primers directed to the flanking exons. The first two coding exons were used in these experiments.

(P) Quantitative evaluation of photoreceptor features in control and morphant animals. All values are percentages. Ex1–3 refer to three independent experiments. The right-most two columns provide the percentage of cells that display triangle-shaped synaptic termini and an area of weaker staining intensity in the inner segment. Morpholino treatment is described in the left-most column.

(Q) A graphic representation of selected data from (P). Photoreceptor inner segment lengths are shortened in *crb2b* ATG and SP morphants and are rescued by mRNA injection. Measurements were performed on both confocal images (left) and electron micrographs (right). "n" and "m" are defined in (F). Error bars indicate standard deviations.

In (B)–(N), apical cell termini are up. C-MO, control morpholino; ATG-MO, ATG-directed morpholino; SP-MO, splice-site directed morpholino. Arrowheads indicate the outer limiting membrane. Asterisk indicates the lens. Additional data are presented in Figures S5 and S6.

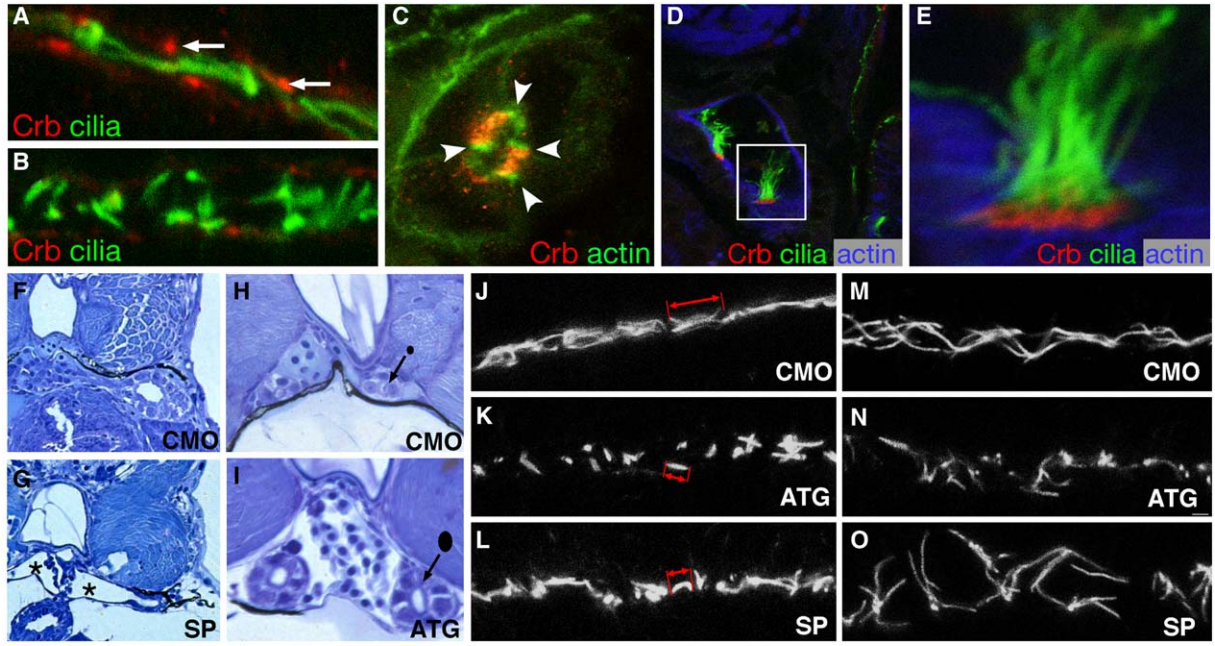

P

	Cyst %	length %		frequency Hz	
		Ex1	Ex2	Ex1	Ex2
C-MO	1 (2/185)	100±15 (15)	100±22 (60)	34±4 (5)	39±3 (16)
ATG-MO	58 (78/133)	38±20 (15)	55±25 (60)	30±1 (5)	34±3 (20)
SP-MO	65 (137/210)	53±17 (15)	68±29 (60)	26±5 (5)	33±4 (20)
SP-MO +mRNA	15 (8/52)	-	93±24 (60)	-	-

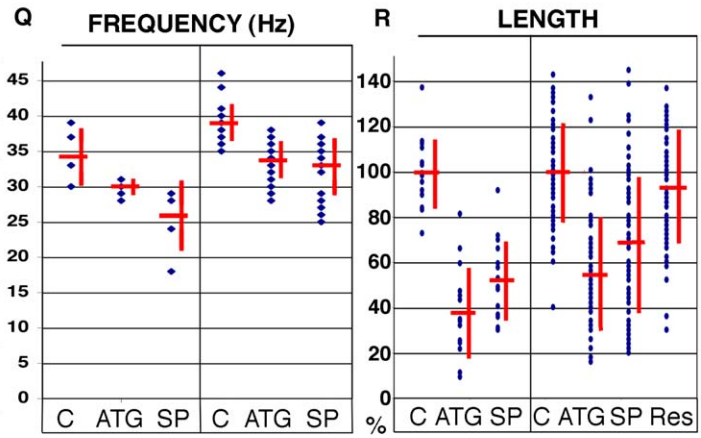

Figure 4. *Crb2b* Is a Determinant of Cilia Length and Motility in Nephric Epithelia

(A and B) Longitudinal optical sections through the zebrafish pronephros stained for Crumbs (red) and acetylated-α-tubulin (green) to visualize cilia at 24 hpf. Crumbs is expressed in a subset of wild-type cells ([A], arrows). In *crb2b* morphants, Crb staining decreases significantly (B).

(C) A transverse section through the nephric duct immunostained for Crumbs (red) and counterstained with phalloidin (green) to visualize actin bundles at 5 dpf. A subset of epithelial cells contains Crumbs at the apical surface. Arrowheads point to apical cell junctions.

(D) A transverse section through the nephric duct at 4 dpf stained for Crumbs (red), filamentous actin (blue), and acetylated α-tubulin (green). A subset of cells feature a dense tuft of apical cilia and display intense Crumbs signal at the apical surface.

(E) Enlargement of a Crb-positive cell (enclosed by a box in [D]).

(F and G) Transverse plastic sections reveal dilation of pronephric tubules (asterisks) in embryos treated with *crb2b*-SP morpholino (G), but not in control morpholino-treated animals (F) at 4 dpf.

(H and I) Transverse plastic sections reveal a dilation of the pronephric duct (arrow) in embryos treated with *crb2b*-ATG morpholino (I), as compared to control animals (H) at 4 dpf. Black circles next to arrows illustrate the approximate size of duct lumen.

(J–O) Cilia of pronephric ducts visualized with an anti-acetylated α-tubulin antibody at 24 hpf in the posterior (J–L) and the anterior (M–O) pronephric duct. *crb2b*-ATG (K, N) and *crb2b*-SP (L, O) morphants feature shorter and mispositioned cilia, compared to control embryos (J, M).

(P–R) The quantitation of differences between *crb2b* morphants and control larvae. Morphants frequently display kidney cysts (P). Cilia are shorter (P, R) and their movement is slower (P, Q) in morphant larvae. Sample sizes are enclosed by parentheses in (P). The length of cilia in (P) was measured in arbitrary units for comparative purposes only and is expressed as the percentage of the control value. The frequency of cilia movement is provided in Hz. In (P)–(R), two independent experiments are presented. In (F)–(I), dorsal is up. ATG, ATG-targeted morpholino; SP, splice site-targeted morpholino; CMO, control morpholino. Additional data are presented in Figure S7.

(Q and R) Error bars indicate standard deviations.

cilia further. Interestingly, the pronephric cilia of morphant animals are shortened and abnormally positioned, so that their axes are frequently perpendicular to the pronephric duct wall (Figures 4M–4O and Movies S7 and S8). The abnormal orientation of cilia may be due to defects in their structure, or, alternatively, it may be a consequence of the fact that dilated pronephric lumen no longer constrains their position. At 24 hpf, the *crb2b* morphant cilia are, on average, ~50% shorter, compared to these in control morpholino-treated animals

(Figures 4J–4P and 4R). This defect is rescued by the injection of *crb2b* mRNA (Figures 4P and 4R). These observations indicate that *crb2b* is required for the differentiation of pronephric cilia and the morphogenesis of the pronephric duct.

One possible cause of pronephric tubule and duct defects could be a loss of apico-basal polarity in the pronephric duct epithelium. To investigate whether or not this is the case, we analyzed transverse sections through morphant pronephric ducts by electron microscopy. Although pronephric ducts are dilated, no defects are obvious in the appearance of cell junctions or apical microvilli of pronephric duct epithelium in morphant animals (Figure S7B, compare to Figure S7A). Similarly, multiciliated cells, which express Crumbs at a high level, do not display obvious defects in the ultrastructure of junctions or cilia (Figure S7D, compare to Figure S7C). To further investigate apico-basal polarity of pronephric epithelia, we stained transverse sections through the pronephros with an antibody to the endosomal protein, Rab5. In both morphants and control morpholino-treated animals, Rab5 localizes to the apical region of the cytoplasm (Figure S7F, compare to Figure S7E). These results indicate that *crb2b* is not necessary for the formation of major features of apico-basal polarity in pronephric epithelia.

To investigate whether *crb2b* function is necessary for cilia motility, we prepared high-speed video recordings of cilia movement in morphant animals. In control morpholino-treated larvae, cilia move in a coordinated fashion, and when viewed in slow motion appear to form a sinusoidal wave (Movies S5 and S6). In contrast to that, after anti-*crb2b* ATG or SP morpholino treatment, ~30% of animals display clearly uncoordinated movement of cilia in severely dilated kidney ducts (Movies S7 and S8). Consistent with antibody staining results (Figures 4J–4O), morphant cilia frequently rotate around axes perpendicular to the pronephric duct wall. The frequency of cilia movement in morphants is reduced by ~10%–20% compared to control larvae (Figure 4Q). These results indicate that *crb2b* is necessary for the normal elongation of pronephric cilia and their position relative to the epithelial surface, as well as their motility.

crb3a Functions in the Elongation of Auditory Kinocilia

In contrast to other Crumbs-family members, Crb3 polypeptides feature very short extracellular domains. Whether or not their function is different from Crb1 or Crb2 is not clear, due to the lack of known genetic defects in *crb3* loci. The *crb3a* transcript is strongly expressed throughout the otic vesicle (Figures S2J–S2L), while the Crumbs polypeptide is detectable at a high level in tether cells only (Figures 5A and 5A′), which are thought to represent hair cell precursors [24]. Other cells of the otic vesicle display much lower, if any, immunoreactivity. The auditory hair cell differentiates two prominent apical features: the microtubule-rich kinocilium (Figures 5B–5D; green signal) and a bundle of villi, which are referred to as stereocilia (Figure 5C, arrow, blue). As ear development progresses, Crumbs remains enriched at the apical termini of hair cells (Figures 5B and 5C), and, curiously, in adult animals it is found mostly at the basal bodies of hair cell kinocilia (Figures 5D and 5D′, arrowheads). To test the role of *crb3a* in auditory hair cells, we performed morpholino knockdown of this gene (Figure S8D). After SP morpholino knockdown, wild-type *crb3a* transcript is no longer detectable by RT-PCR (Figure S8D), and Crumbs expression in hair cells is reduced or absent. The kinocilia of morphant animals are shortened by ~15% and 30% for ATG and SP morpholinos, respectively (Figures 5F, 5G, 5I; Figure S8A). This difference is not caused by a general distortion of ear morphology, as the length of hair cell somata remains unchanged (Figures S8A and S8C). Phalloidin staining does not reveal obvious structural defects in morphant stereocilia, indicating that the shortening of kinocilia is not a consequence of a general apical surface defect (not shown). As the length of kinocilia is roughly the same at 36 and 48 hpf in control animals (Figure 5H, Figure S8B), their shortening in morphants is unlikely to result from a developmental delay. This analysis indicates that *crb3a* function regulates the length of auditory kinocilia.

Contrary to what *crb3a* transcript expression would suggest, its knockdown does not produce any obvious defect in the apico-basal polarity of the otic vesicle epithelium. To further test its role in epithelial polarity, we overexpressed *crb3a* in the otic vesicle with a Tol-2 transposon-based vector equipped with a heat-shock promoter (Figure 5M). In addition to providing means for the temporal control of expression, this approach produces a higher expression level than mRNA injection (Figure S9D, compare to Figure S9B). *crb3a* expression was induced by elevated temperature at 22 and 26 hpf. No defects of epithelial polarity are obvious following this treatment at 32 hpf (Figures 5J and 5J′), and the length of kinocilia remains unaltered (data not shown). Interestingly, the same procedure induces profound epithelial polarity defects in the retinal neuroepithelium (Figures 5K and 5L), including a displacement of apical junctions (Figure 5L, arrowheads), as well as the loss of apical determinants, such as Has/aPKC, from the apical surface (data not shown). At later stages of development, this phenotype is followed by a severe disorganization of retinal architecture that closely resembles the phenotype of *ome* mutant embryos (Table S2, and data not shown). These experiments corroborate the role of *crumbs* genes in apico-basal polarity of neuroepithelia and indicate that although both retinal and otic vesicle epithelia express *crumbs* transcripts, the apico-basal polarity of these tissues is regulated by different mechanisms. Furthermore, they show that Crb3 polypeptides are able to interact with apico-basal polarity pathways in tissues that express *crb2*-type genes, suggesting functional similarity between *crumbs* loci.

crb Genes Are Functionally Interchangeable

Experiments in *Drosophila* revealed that Crumbs function in embryonic epithelia is largely, if not entirely, mediated by its cytoplasmic tail [25]. As the cytoplasmic tails of zebrafish *crb* genes share high sequence similarity (Figure 1I), we hypothesized that vertebrate genes may be functionally interchangeable in at least some aspects of embryonic development. To test this idea, we attempted to rescue the *ome* mutant phenotype by the injection of *crb2b* mRNA. Phenotypic rescue was scored both on the basis of eye pigmentation and the formation

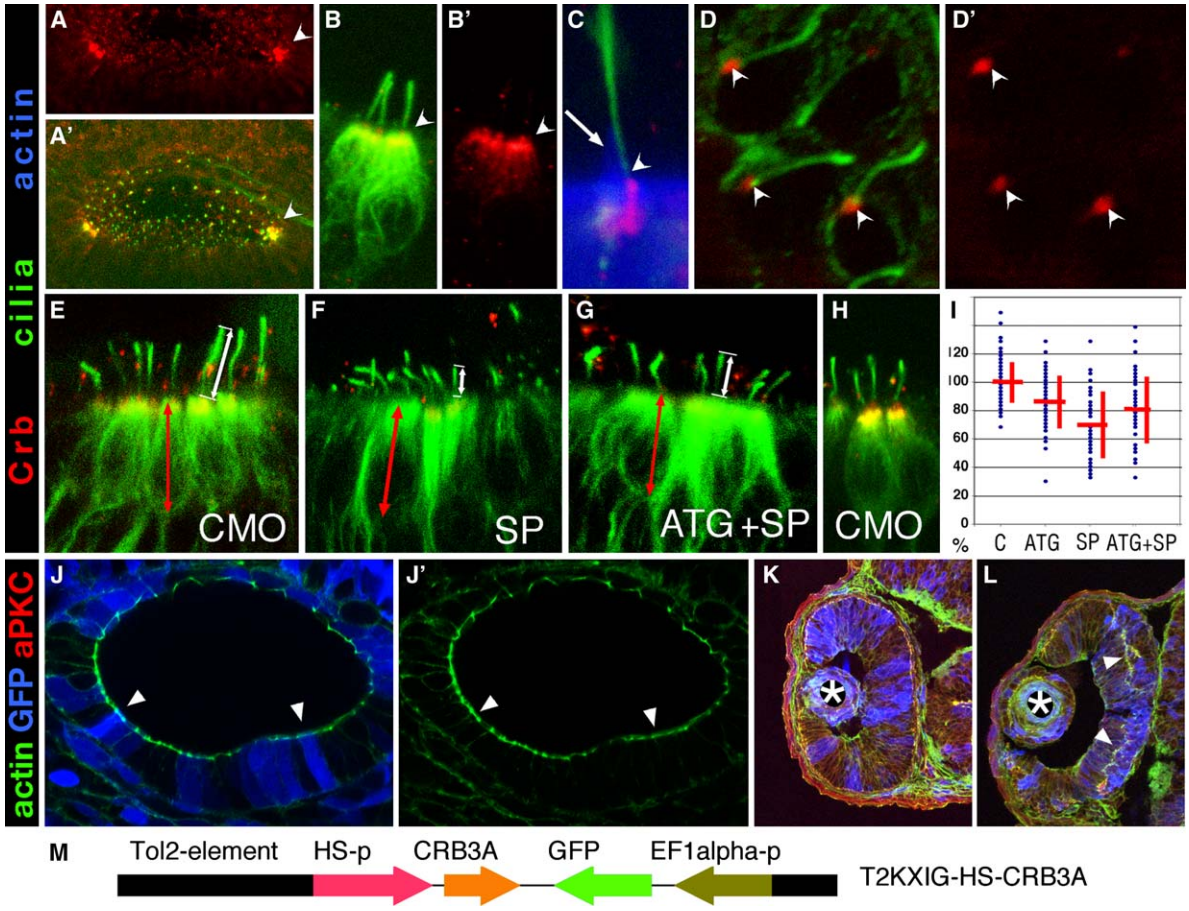

Figure 5. *crb3a* Function in the Auditory System

(A, A′) The otic vesicle of wild-type zebrafish larvae stained with antibodies to Crumbs (red) and acetylated α-tubulin (green) at 24 hpf. Crumbs signal is highly elevated in tether cells (arrowheads).

(B, B′) Tether cells stained as above at 30 hpf. Crumbs is highly enriched at their apical termini (arrowhead).

(C) A hair cell stained to visualize acetylated α-tubulin (green), Crumbs (red), and actin bundles (blue) at 72 hpf. Crumbs polypeptide localizes to the apical termini of hair cells (arrowhead). Arrow indicates stereociliary bundle.

(D, D′) Surface view of a sensory macula in the adult zebrafish ear stained as in (A). Crumbs staining (red) is highly elevated at the bases (arrowheads) of hair cell kinocilia (green).

(E–G) Optical sections through anterior auditory maculae of zebrafish treated with a control morpholino (E), an SP morpholino (F), and a mix of ATG and SP morpholinos (G). Whole larvae were stained at 48 hpf as in (A). The lengths of cilia and hair cell somata were measured as indicated with white and red arrows, respectively.

(H) Hair cells of control morpholino-treated animals visualized as above at 36 hpf.

(I) The length of kinocilia in morpholino-treated zebrafish larvae at 48 hpf. Error bars indicate standard deviations.

(J, J′) The otic vesicle stained with phalloidin (green) to visualize apical cell junctions at 32 hpf. In (J), GFP-positive cells (blue) overexpress *Crb3a*. No ectopic junctions are observed.

(K and L) At 32 hpf, ectopic adherens junction-associated actin bundles are observed in retinae overexpressing *crb3a* ([L], arrowheads) but not in control eyes, which express GFP alone (K). GFP staining (blue) identifies cells that overexpress *crb3a*, actin is in green, and asterisks indicate the lens.

(M) A schematic representation of the Tol2-transposon-based overexpression vector. HS-p and EF1α-p are heat shock and elongation factor 1α promoters, respectively.

Length measurements in (I) are expressed as the percentage of the control value. C or CMO, control morpholino; ATG, ATG-directed morpholino; SP, splice site-directed morpholino. Additional data are presented in Figures S8 and S9.

of correct neuronal layering. The injection of *crb2b* mRNA into *ome* mutant homozygotes rescues both eye pigmentation and neuronal architecture (Table S1). More importantly, the injection of *crb3a* mRNA, which encodes only a rudimentary extracellular domain, also rescues the *ome* mutant phenotype. The strength of rescue is similar for *ome*, *crb2b*, and *crb3a* mRNA. In all three cases, eye pigmentation is normal in 95% of embryos or more, and two distinct plexiform layers form in correct positions in 40%–70% of rescued animals (Table S1 and Figures 6A–6L). We note that in all rescue experiments, including that by *ome* mRNA injection, the retina is not entirely normal, and some ectopic photoreceptors persist outside the photoreceptor cell layer. This is not surprising, as mRNA injection does not reproduce the native expression pattern. These observations strongly suggest that the C-terminal portion of Crumbs proteins is sufficient to mediate many, if not all, of *ome*

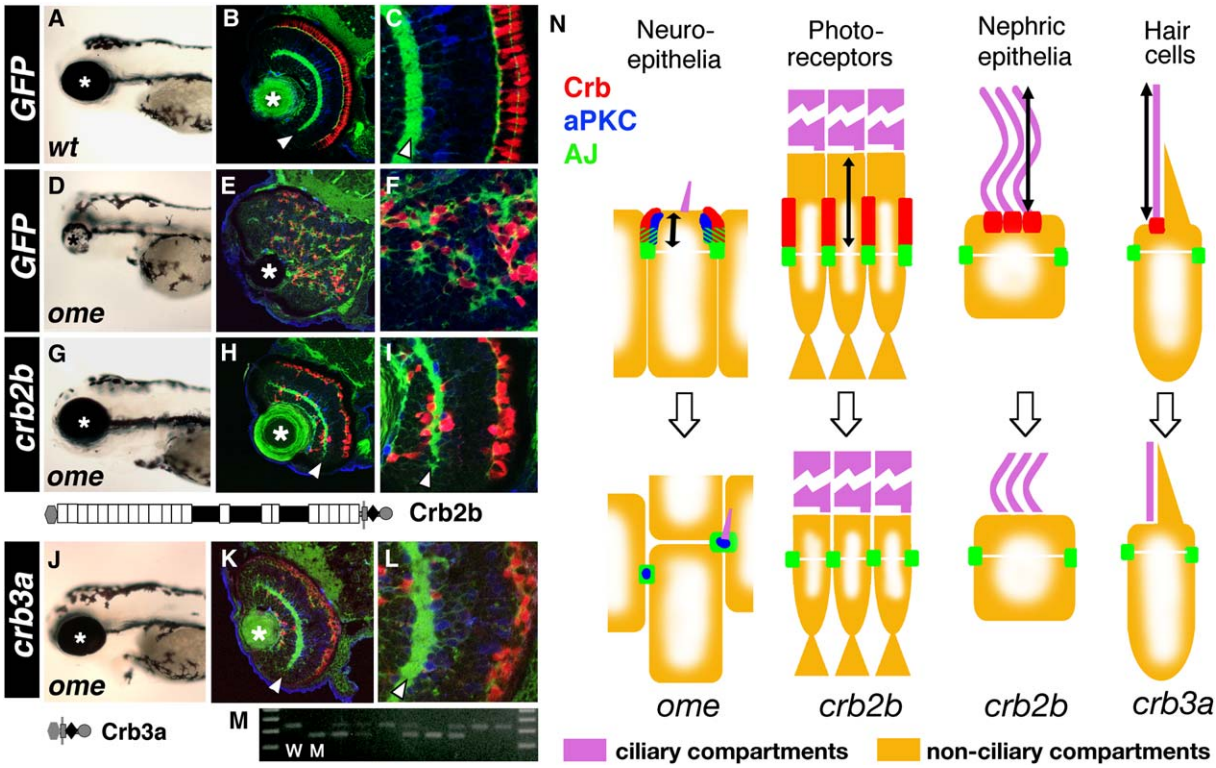

Figure 6. *crumbs* Genes Are Functionally Interchangeable

(A–L) External phenotypes (left column) and retinal architecture (center and right columns) of wild-type (A–C) or *ome* homozygous mutant (D–L) larvae treated with GFP (A–F), *crb2b* (G–I), or *crb3a* (J–L) mRNA. Sections are stained with phalloidin to visualize plexiform layers (green), the zpr-1 antibody to detect double cones (red), and anti-carbonic anhydrase antibody to label radial glia (blue).

(M) Electrophoresis of the PCR amplification product of the SSLP polymorphism, AL-91K, was used to genotype larvae in rescue experiments.

(N) A schematic diagram of phenotypic changes in mutants and morphants of *ome* and its paralogs. Crb proteins (red) localize to apical structures such as the cell surface in the vicinity of neuroepithelial cell junctions, the inner segment of photoreceptors, and the basal region of cilia. Adherens junctions are shown in green. In *ome* mutants, aPKC staining (blue) and most cilia are found in the vicinity of ectopic junctional complexes. The apical surface of photoreceptors (inner segment) and the cilia of selected cells in the auditory and pronephric system are reduced in size. In (A)–(L), asterisks indicate the lens and arrowheads the inner plexiform layer. The structures of the Crb2b and Crb3a polypeptides are depicted schematically below (G) and (J), respectively. In left-most panels, dorsal is up, anterior is left. W, wild-type; M, mutant.

developmental functions in apico-basal polarity and in the formation of retinal architecture. To further test the idea that *crumbs* genes are functionally interchangeable, we injected *ome* mRNA along with *crb2b* morpholinos into zebrafish embryos. This treatment rescues the kidney phenotype as well as the shortening of inner segments of *crb2b* morphants (Table S3). These results indicate that *crumbs* genes can substitute for each other in at least some developmental processes, and thus share key functional characteristics.

Discussion

Prior to our studies in zebrafish, *crumbs* genes have been the subject of analysis in the mouse. Two mutant alleles, one spontaneous and one targeted, are available for *Crb1* gene in the mouse—both are likely to induce the null phenotype [26, 27]. Neither of them, however, produces a developmental defect, perhaps due to genetic redundancy [27]. Nonetheless, in juvenile animals, *Crb1* deficiency results in a progressive photoreceptor loss. This is consistent with the findings that human *CRB1* mutations lead to several forms of hereditary blindness, including retinitis pigmentosa and Leber's congenital amaurosis [28]. In agreement with mouse and human studies, our attempts to knock down *crb1* function in wild-type or *ome* mutant zebrafish have failed to produce an obvious embryonic phenotype (data not shown). In contrast to that, the genetic manipulations of *ome*, *crb2b*, or *crb3a* produce a reduction or the loss of apical surface features and are frequently associated with severe morphological defects in the developing embryo.

Mutations in *nok*, *moe*, and *has* genes are known to produce phenotypes similar to *ome* defect in retina [11, 13, 15, 18, 29]. To investigate whether mutants of these loci also display cilia defects similar to the ones observed in *crb2b* and *crb3a* morphants, we measured cilia length in the pronephros and the otic vesicle. This analysis did not reveal any obvious mutant phenotypes (data not shown). At least two scenarios may account for the absence of ciliary defects in these mutant strains. First, *crumbs* function in ciliogenesis may be mediated by mechanisms that do not involve *nok* or *has* genes. Second, redundant genetic pathways may obscure the role of these loci. Indeed, two *nok* paralogs appear to be present in the zebrafish genome (M. Tsujikawa and J.M., unpublished data).

crb Function in Epithelial Polarity

The loss of apico-basal polarity in the neuroepithelial primordium of the *ome* retina is followed by a severe disorganization of neuronal architecture in the differentiated eye [13]. This phenotype can be explained by at least two scenarios. First, it may be a result of neuroepithelial polarity defect, which is likely to affect neuronal migration patterns in a cell-nonautonomous manner; second, it may reflect a cell-autonomous function of *ome* in postmitotic neuronal precursors. Protein expression pattern argues against the possibility that *ome* functions in postmitotic neurons. Crumbs polypeptides are not detectable in the ganglion cell layer and are present in only a small subpopulation of neurons in the inner nuclear layer (not shown) and thus are rather unlikely to affect the pattern of postmitotic neurons in a cell-autonomous manner. Although we cannot entirely exclude the possibility that a small amount of Crumbs polypeptide is present in migrating neuronal precursors, our data suggest that the apico-basal polarity of the neuroepithelium is a prerequisite for the formation of neuronal architecture in the central nervous system.

Photoreceptors and epithelial cells share several characteristics. Perhaps the most obvious of these is the subdivision of their surface into two domains by a belt of cell junctions [22]. The determinants of cell polarity, such as Nok, Has, and Pard3, are enriched apical to cell junctions and are absent from the basal region in photoreceptors and epithelial cells alike, indicating that the molecular identity of the apical membrane compartment is similar in both cell classes [4, 11, 14, 27, 30]. Also, Crumbs immunoreactivity localizes apically in photoreceptor cells (Figure 3). Given this distribution, we hypothesized that *crb2b* regulates the formation of photoreceptor apical membrane. This indeed appears to be the case, as *crb2b* knockdown produces a dramatic reduction of the inner segment size, while many other photoreceptor cell features remain intact. In contrast to these results, the genetic defects of mouse *Crb1* produce a late-onset loss of OLM junctions and focal changes of photoreceptor morphology, which may or may not be secondary to cell degeneration [26, 27]. Thus, based on our studies, vertebrate *crumbs* genes function in photoreceptor morphogenesis, and not only in photoreceptor survival. The *crb2b* knockdown phenotype in zebrafish is similar to the reduction of rhabdomeric membrane stalk in *crumbs* fly mutants [4], indicating that the genetic mechanisms responsible for photoreceptor membrane polarity are conserved between flies and mammals.

crb Function in Cilia

The apical cell membrane forms extensions, such as cilia or villi. In some cells, apical cilia differentiate into complex structures, such as outer segments of vertebrate photoreceptor cells [22]. In other tissues, cilia are motile and their movement propagates fluid flow [31, 32]. The protein composition of the ciliary membrane is different from the rest of the apical surface, and hence the cilium can be thought of as a separate membrane compartment [8]. Our analysis reveals that both in the ciliary and the nonciliary portion of the apical cell membrane, the loss of *crumbs* function results in the same phenotype: the reduction of membrane area. It is not clear at this point what mechanism is responsible for the shortening of cilia. In one possible scenario, *crumbs* could be necessary for the normal occurrence of intraflagellar transport (IFT). Alternatively, *crumbs* could influence cilia elongation by directly regulating the size of the ciliary membrane. Such a scenario would be consistent with its function in the nonciliary compartment, such as the photoreceptor inner segment, where IFT is clearly of little relevance to apical membrane size.

A frequent characteristic of *crumbs* phenotypes is a reduction of apical membrane size in either ciliary or nonciliary compartments (summarized in Figure 6N). This phenotype is not obvious in the retinal neuroepithelium, possibly due to mechanical constraints in this tissue, which favor the loss of epithelial integrity and a displacement of fragmented junctional complexes to more basal locations. Common functional features of *crumbs* genes are consistent with the conservation of their cytoplasmic tails and with the observation that in the *ome* mutant rescue assay, *crb2b* and *crb3a* are as effective as *ome* itself. It is particularly striking that *crb3a*, a determinant of cilia length that is enriched at the base of hair cell kinocilia, can substitute for at least some, or possibly all, functions of *ome* in retinal patterning. This result implies that *crb3a* successfully interacts with the molecular machinery that mediates *ome* function. These results support the idea that the same *crumbs*-dependant mechanism of membrane size determination operates in both ciliary and nonciliary compartments. Although we find it presently less appealing, our data do not exclude an alternative scenario that ciliary and nonciliary functions of *crumbs* are unrelated to each other.

Conclusions

Highly polarized cells, such as those that form epithelial sheets, frequently display a subdivision of their surface into apical and basolateral membrane compartments and often develop specializations at their apical surface. One of the most common apical features of these cells is the presence of cilia or their derivatives. We show that zebrafish *oko meduzy* (*ome*) locus encodes a *crumbs* homolog, essential for the proper apico-basal polarity of neural tube neuroepithelium. *ome* paralogs *crb2b* and *crb3a* promote the formation of apical cell features: photoreceptor inner segments and cilia in the renal as well as auditory system. Apical surface defects in *ome*- and *crb2b*-deficient animals are associated with profound disorganization of neuronal architecture and with the formation of pronephric cysts, respectively. In addition, we show that despite differences in their structure and expression patterns, *crumbs* genes are largely functionally interchangeable. Thus, vertebrate *crumbs* genes play key roles in many aspects of apical surface differentiation, including the positioning of cell junctions, the determination of apical membrane size, and the elongation of cilia.

Experimental Procedures

Fish Strains and Histology

The maintenance and breeding of zebrafish strains as well as the staging of embryonic development were performed as described previously [33, 34]. The ome^{m98} and ome^{m289} alleles were originally recovered in the course of a large-scale mutagenesis screen [18]. The external phenotypes of embryos and larvae were recorded as

described in our previous studies ([23] and references therein). The preparation of plastic and frozen sections as well as electron microscopy were performed as previously [23].

Cloning, Morpholino Knockdown, and Phenotypic Rescue

To map the *ome* locus, F2 embryos from a cross between heterozygous carriers of the ome^{m289} allele (AB genetic background) and wild-type WIK strain homozygotes were genotyped as described previously [21]. cDNAs of *ome* and its paralogs were isolated via the RACE procedure, with GeneRacer Kit (Invitrogen). For these experiments, total RNA was extracted from embryos with Trizol regent at 3 dpf (Invitrogen). Mutations were detected by direct sequencing of PCR products amplified from both genomic DNA and cDNA. GenBank accession numbers are as follows: *crb1*, DQ314735; *ome*, DQ314736; *crb2b*, DQ314737; *crb3a*, DQ314738; and *crb3b*, DQ314739.

In knockdown experiments, morpholino-modified oligonucleotides (morpholinos) were reconstituted in 120 mM KCl and injected into the yolk of wild-type AB embryos at the 1- to 2-cell stage as described previously [34]. The following morpholinos were used: *ome*-ATG, CAGATGCACTTTCCTGATCTCCATG; *ome*-SP, ACGTTGCCA GTACCTGTGTATCCTG; *crb2b*-ATG, ACATCCGTCCAAAATCCATG TCCTG; *crb2b*-SP, TAAAGATGTCCTACCCAGCTTGAAC; *crb3a*-ATG, AGCCCAACCTGCTGGATCATTTCCG; *crb3a*-SP, ACTGACTC ACCCTGTGCCGAAACAT.

To rescue the *ome* phenotype, the full-length *ome*, *crb2b*, and *crb3a* coding sequences were cloned into the pXT7 vector (see Figure 1 in [34]) and their identity was confirmed by sequencing. Transcription reactions were performed with mMessage mMachine kit (Ambion Inc.), according to manufacturer's instructions. Approximately 40 pg of RNA was injected into embryos at the 1-cell stage. To identify genotypically mutant animals, embryos were cut in half. The caudal halves were used to extract DNA and to PCR amplify the AL-91K polymorphism, which was subsequently genotyped by agarose gel electrophoresis. The front halves of embryos were sectioned to determine retinal architecture.

Immunohistochemistry

Fixation, infiltration, sectioning of embryos, and other steps of antibody staining procedure were described previously [23, 35]. The following primary antibodies and dilutions were used: mouse anti-acetylated-α-tubulin to visualize cilia (1:500, Sigma); Zpr-1 to stain red-green double cones (1:250, Oregon Monoclonal Bank); mouse anti-SV2 to visualize synaptic termini of photoreceptors (1:200, Developmental Studies Hybridoma Bank); rabbit anti-Crb3 to visualize the Crb polypeptides (1:250, gift from Dr. B. Margolis); rabbit anti-aPKC (1:500, C-20, Santa Cruz Biotechnology); rabbit anti-Pard3 (1:100, gift from Dr. D. Hyde); rabbit anti-carbonic anhydrase to visualize the Muller Glia (1:250, gift from Dr. P. Linser); mouse anti-ZO1 (1:50, 1A12, Invitrogen); rabbit anti-β-catenin (1:250, gift from Herbert Steinbeisser) [36]; and rabbit anti-Rab5 (1:50, FL215, Santa Cruz Biotechnology). The anti-Crumbs antibody that we used in our studies was raised against the 20 amino acid long C-terminal peptide of human CRB3 [37]. Since this region is highly conserved in all crumbs genes (Figure 1), this antibody is expected to recognize multiple Crumbs proteins. An antibody generated to human CRB2 (gift from Dr. Rashbass) produces similar, if not identical, staining pattern (data not shown). The staining of hair cell and pronephric cilia was performed as described in previous publications [21, 32].

Videomicroscopy

Cilia motility in the pronephros was analyzed in two independent experiments. In the first test, embryos were placed in methylcellulose on microscope slides; in the second, embryos were immobilized in Petri dishes in low melting point agarose. After that, embryos were filmed with a high-speed Photron FASTCAM-PCI500 digital video camera (Photron LTD) at 250 frames per s for the duration of 1 s. The camera was mounted on an Axioplan microscope (Zeiss Inc.) equipped with a 63× water immersion lens. To stop the heartbeat and circulation, 40 mmol/l BDM (2,3-butanedione monoxime, Sigma) was added to egg water ~1 min prior to video recording.

In Situ Hybridization

Partial nucleotide sequences of *crb1, ome, crb2b, crb3a,* and *crb3b* were amplified by RT-PCR and cloned into pCRII-TOPO vector (Invitrogen). The following primers were used for amplification: CATTC ACCTCAATCTCGCAGAGCT and CCATCTGTGGCGATGAACAGCA GA for *crb1*, TGCCACATCGTCTTGGAAAAGTCA and TACCCACCA CTAAAGTGTGCCCTG for *ome*, TTCAGCACGCTGCCCATCTCCATT and TCCTCCTCGTGAGTGTGATGT for *crb2b*, GGTTGAGGGTAGA GGTGCAGATTG and AGGGATTGAGTCACCATTATCACG for *crb3a*, and AGGATGTTCAAGCTCTTCCCAGGT and CTCATTAACTCAAAG AATGGTGTGC for *crb3b*. Probe preparation, hybridization, washes, signal detection, and data recording procedures were carried out with standard protocols ([23] and references therein).

Heat Shock-Induced Overexpression of *crb3a*

In the *crb3a* overexpression vector, the full-length *crb3a* cDNA is inserted between hsp70 promoter, derived from the pXT7-HS-GFP construct [34], and the SV40 polyadenylation site. The above cassette is inserted between the Bgl II and Cla I restriction sites in the T2KXIG vector [38], replacing the GFP polyA region. The injection of this construct into embryos was performed as described previously [38]. Heat shock treatment was accomplished by incubating embryos at 37°C for 1 hr at 22 hpf and 26 hpf.

Supplemental Data

Supplemental Data include nine figures, three tables, eight movies, and Supplemental Experimental Procedures and can be found with this article online at http://www.current-biology.com/cgi/content/full/16/10/945/DC1/.

Acknowledgments

We thank Dr. Tepass for anti-Crb1 antibody, Dr. Rashbass for anti-Crb2 antibody, Dr. Margolis for anti-Crb3 antibody, Dr. Steinbeisser for anti-β-catenin antibody, Drs. Hyde and Wei for the anti-Pard3 antibody, and Dr. Kawakami for the Tol2 transposon vector. Dr. John Mably kindly shared his expertise in the preparation of high-speed videorecordings, and Aletta Schnitzler provided help during early efforts to map the *ome* locus. Drs. Christopher Walsh, Liliana Solnica-Krezel, Francesca Pignoni, and Arindam Majumdar provided many helpful comments on the earlier versions of this manuscript. We also thank Dr. Motokazu Tsujikawa for useful suggestions and Andrei Avanesov and Andria Schibler for excellent technical assistance. These studies were supported by the NEI RO1 EY11882 and EY016859 awards (to J.M.), the NIDCD RO1 DC005103 award (to J.M.), a Knights Templar Pediatric Ophthalmology research grant (to Y.O.), and a core grant for Vision Research P30EY14104 to the Harvard Department of Ophthalmology.

Received: November 1, 2005
Revised: February 26, 2006
Accepted: March 13, 2006
Published: May 22, 2006

References

1. Kemphues, K.J., Kusch, M., and Wolf, N. (1988). Maternal-effect lethal mutations on linkage group II of *Caenorhabditis elegans*. Genetics *120*, 977–986.
2. Wieschaus, E., Nusslein-Volhard, C., and Jergens, G. (1984). Mutations affecting the pattern of the larval cuticle in *D. melanogaster*. Rouxs Arch. Dev. Biol. *193*, 296–307.
3. Jurgens, G., Wieschaus, E., Nusslein-Volhard, C., and Kluding, C. (1984). Mutations affecting the pattern of the larval cuticle in *Drosophila melanogaster*. Rouxs Arch. Dev. Biol. *193*, 283–295.
4. Pellikka, M., Tanentzapf, G., Pinto, M., Smith, C., McGlade, C.J., Ready, D.F., and Tepass, U. (2002). Crumbs, the *Drosophila* homologue of human CRB1/RP12, is essential for photoreceptor morphogenesis. Nature *416*, 143–149.
5. Izaddoost, S., Nam, S.C., Bhat, M.A., Bellen, H.J., and Choi, K.W. (2002). *Drosophila* Crumbs is a positional cue in photoreceptor adherens junctions and rhabdomeres. Nature *416*, 178–183.

6. Grawe, F., Wodarz, A., Lee, B., Knust, E., and Skaer, H. (1996). The *Drosophila* genes *crumbs* and *stardust* are involved in the biogenesis of adherens junctions. Development *122*, 951–959.
7. Hong, Y., Stronach, B., Perrimon, N., Jan, L.Y., and Jan, Y.N. (2001). *Drosophila* Stardust interacts with Crumbs to control polarity of epithelia but not neuroblasts. Nature *414*, 634–638.
8. Rosenbaum, J.L., and Witman, G.B. (2002). Intraflagellar transport. Nat. Rev. Mol. Cell Biol. *3*, 813–825.
9. Fan, S., Hurd, T.W., Liu, C.J., Straight, S.W., Weimbs, T., Hurd, E.A., Domino, S.E., and Margolis, B. (2004). Polarity proteins control ciliogenesis via kinesin motor interactions. Curr. Biol. *14*, 1451–1461.
10. Malicki, J. (2000). Harnessing the power of forward genetics—analysis of neuronal diversity and patterning in the zebrafish retina. Trends Neurosci. *23*, 531–541.
11. Horne-Badovinac, S., Lin, D., Waldron, S., Schwarz, M., Mbamalu, G., Pawson, T., Jan, Y., Stainier, D.Y., and Abdelilah-Seyfried, S. (2001). Positional cloning of *heart and soul* reveals multiple roles for PKC lambda in zebrafish organogenesis. Curr. Biol. *11*, 1492–1502.
12. Masai, I., Lele, Z., Yamaguchi, M., Komori, A., Nakata, A., Nishiwaki, Y., Wada, H., Tanaka, H., Nojima, Y., Hammerschmidt, M., et al. (2003). N-cadherin mediates retinal lamination, maintenance of forebrain compartments and patterning of retinal neurites. Development *130*, 2479–2494.
13. Malicki, J., and Driever, W. (1999). *oko meduzy* mutations affect neuronal patterning in the zebrafish retina and reveal cell-cell interactions of the retinal neuroepithelial sheet. Development *126*, 1235–1246.
14. Wei, X., and Malicki, J. (2002). *nagie oko*, encoding a MAGUK-family protein, is essential for cellular patterning of the retina. Nat. Genet. *31*, 150–157.
15. Jensen, A.M., and Westerfield, M. (2004). Zebrafish mosaic eyes is a novel FERM protein required for retinal lamination and retinal pigmented epithelial tight junction formation. Curr. Biol. *14*, 711–717.
16. Malicki, J., Jo, H., and Pujic, Z. (2003). Zebrafish N-cadherin, encoded by the *glass onion* locus, plays an essential role in retinal patterning. Dev. Biol. *259*, 95–108.
17. Driever, W., Solnica-Krezel, L., Schier, A.F., Neuhauss, S.C., Malicki, J., Stemple, D.L., Stainier, D.Y., Zwartkruis, F., Abdelilah, S., Rangini, Z., et al. (1996). A genetic screen for mutations affecting embryogenesis in zebrafish. Development *123*, 37–46.
18. Malicki, J., Neuhauss, S.C., Schier, A.F., Solnica-Krezel, L., Stemple, D.L., Stainier, D.Y., Abdelilah, S., Zwartkruis, F., Rangini, Z., and Driever, W. (1996). Mutations affecting development of the zebrafish retina. Development *123*, 263–273.
19. Roh, M.H., Makarova, O., Liu, C.J., Shin, K., Lee, S., Laurinec, S., Goyal, M., Wiggins, R., and Margolis, B. (2002). The Maguk protein, Pals1, functions as an adapter, linking mammalian homologues of Crumbs and Discs Lost. J. Cell Biol. *157*, 161–172.
20. Klebes, A., and Knust, E. (2000). A conserved motif in Crumbs is required for E-cadherin localisation and zonula adherens formation in *Drosophila*. Curr. Biol. *10*, 76–85.
21. Tsujikawa, M., and Malicki, J. (2004). Intraflagellar transport genes are essential for differentiation and survival of vertebrate sensory neurons. Neuron *42*, 703–716.
22. Rodieck, R.W. (1973). The Vertebrate Retina. Principles of Structure and Function (San Francisco: W.H. Freeman & Co).
23. Avanesov, A., and Malicki, J. (2004). Approaches to study neurogenesis in the zebrafish retina. Methods Cell Biol. *76*, 333–384.
24. Riley, B.B., Zhu, C., Janetopoulos, C., and Aufderheide, K.J. (1997). A critical period of ear development controlled by distinct populations of ciliated cells in the zebrafish. Dev. Biol. *191*, 191–201.
25. Wodarz, A., Hinz, U., Engelbert, M., and Knust, E. (1995). Expression of crumbs confers apical character on plasma membrane domains of ectodermal epithelia of *Drosophila*. Cell *82*, 67–76.
26. Mehalow, A.K., Kameya, S., Smith, R.S., Hawes, N.L., Denegre, J.M., Young, J.A., Bechtold, L., Haider, N.B., Tepass, U., Heckenlively, J.R., et al. (2003). CRB1 is essential for external limiting membrane integrity and photoreceptor morphogenesis in the mammalian retina. Hum. Mol. Genet. *12*, 2179–2189.
27. van de Pavert, S.A., Kantardzhieva, A., Malysheva, A., Meuleman, J., Versteeg, I., Levelt, C., Klooster, J., Geiger, S., Seeliger, M.W., Rashbass, P., et al. (2004). Crumbs homologue 1 is required for maintenance of photoreceptor cell polarization and adhesion during light exposure. J. Cell Sci. *117*, 4169–4177.
28. den Hollander, A.I., ten Brink, J.B., de Kok, Y.J., van Soest, S., van den Born, L.I., van Driel, M.A., van de Pol, D.J., Payne, A.M., Bhattacharya, S.S., Kellner, U., et al. (1999). Mutations in a human homologue of *Drosophila* crumbs cause retinitis pigmentosa (RP12). Nat. Genet. *23*, 217–221.
29. Peterson, R.T., Mably, J.D., Chen, J.N., and Fishman, M.C. (2001). Convergence of distinct pathways to heart patterning revealed by the small molecule concentramide and the mutation heart-and-soul. Curr. Biol. *11*, 1481–1491.
30. Wei, X., Cheng, Y., Luo, Y., Shi, X., Nelson, S., and Hyde, D.R. (2004). The zebrafish Pard3 ortholog is required for separation of the eye fields and retinal lamination. Dev. Biol. *269*, 286–301.
31. Okada, Y., Takeda, S., Tanaka, Y., Belmonte, J.C., and Hirokawa, N. (2005). Mechanism of nodal flow: a conserved symmetry breaking event in left-right axis determination. Cell *121*, 633–644.
32. Kramer-Zucker, A.G., Olale, F., Haycraft, C.J., Yoder, B.K., Schier, A.F., and Drummond, I.A. (2005). Cilia-driven fluid flow in the zebrafish pronephros, brain and Kupffer's vesicle is required for normal organogenesis. Development *132*, 1907–1921.
33. Kimmel, C.B., Ballard, W.W., Kimmel, S.R., Ullmann, B., and Schilling, T.F. (1995). Stages of embryonic development of the zebrafish. Dev. Dyn. *203*, 253–310.
34. Malicki, J., Jo, H., Wei, X., Hsiung, M., and Pujic, Z. (2002). Analysis of gene function in the zebrafish retina. Methods *28*, 427–438.
35. Avanesov, A., Dahm, R., Sewell, W.F., and Malicki, J.J. (2005). Mutations that affect the survival of selected amacrine cell subpopulations define a new class of genetic defects in the vertebrate retina. Dev. Biol. *285*, 138–155.
36. Schneider, S., Steinbeisser, H., Warga, R.M., and Hausen, P. (1996). Beta-catenin translocation into nuclei demarcates the dorsalizing centers in frog and fish embryos. Mech. Dev. *57*, 191–198.
37. Makarova, O., Roh, M.H., Liu, C.J., Laurinec, S., and Margolis, B. (2003). Mammalian Crumbs3 is a small transmembrane protein linked to protein associated with Lin-7 (Pals1). Gene *302*, 21–29.
38. Kawakami, K., Takeda, H., Kawakami, N., Kobayashi, M., Matsuda, N., and Mishina, M. (2004). A transposon-mediated gene trap approach identifies developmentally regulated genes in zebrafish. Dev. Cell *7*, 133–144.